

---

# A PHYSICS-INFORMED LOW-SHOT LEARNING FOR SEMG-BASED ESTIMATION OF MUSCLE FORCE AND JOINT KINEMATICS

---

A PREPRINT

✉ **Yue Shi**

School of Electronic and Electrical Engineering,  
The University of Leeds,  
Leeds, UK  
y.shi1@leeds.ac.uk

✉ **Shuhao Ma**

School of Electronic and Electrical Engineering,  
The University of Leeds,  
Leeds, UK  
elsma@leeds.ac.uk

✉ **Yihui Zhao**

Bristol robotic lab,  
University of Bristol,  
Bristol, UK  
yihui.zhao@bristol.ac.uk

✉ **Zhiqiang Zhang**

School of Electronic and Electrical Engineering,  
The University of Leeds,  
Leeds, UK  
z.zhang3@leeds.ac.uk

✉ **Zhiqiang Zhang**

School of Electronic and Electrical Engineering,  
The University of Leeds,  
Leeds, UK

July 12, 2023

## ABSTRACT

Muscle force and joint kinematics estimation from surface electromyography (sEMG) are essential for real-time biomechanical analysis of the dynamic interplay among neural muscle stimulation, muscle dynamics, and kinetics. Recent advances in deep neural networks (DNNs) have shown the potential to improve biomechanical analysis in a fully automated and reproducible manner. However, the small sample nature and physical interpretability of biomechanical analysis limit the applications of DNNs. This paper presents a novel physics-informed low-shot learning method for sEMG-based estimation of muscle force and joint kinematics. This method seamlessly integrates Lagrange's equation of motion and inverse dynamic muscle model into the generative adversarial network (GAN) framework for structured feature decoding and extrapolated estimation from the small sample data. Specifically, Lagrange's equation of motion is introduced into the generative model to restrain the structured decoding of the high-level features following the laws of physics. And a physics-informed policy gradient is designed to improve the adversarial learning efficiency by rewarding the consistent physical representation of the extrapolated estimations and the physical references. Experimental validations are conducted on two scenarios (i.e. the walking trials and wrist motion trials). Results indicate that the estimations of the muscle forces and joint kinematics are unbiased compared to the physics-based inverse dynamics, which outperforms the selected benchmark methods, including physics-informed convolution neural network (PI-CNN), vanilla generative adversarial network (GAN), and multi-layer extreme learning machine (ML-ELM).

**Keywords** muscle force and joint kinematics · surface Electromyographic · low-shot learning · generative adversarial network · physics-informed optimization · mode collapse

## 1 Introduction

Human movements involve complex interactions within the neuromuscular system. The surface electromyography (sEMG)-driven estimation of muscle force and joint kinematics dynamics provides detailed biomechanical analysis to understand the neuromuscular system [Falisse et al.(2019)Falisse, Serrancolí, Dembia, Gillis, Jonkers, and De Groote, Modenese and Kohout(2020)], which benefits various applications, such as sports rehabilitation treatments [Smith et al.(2021)Smith, Coppack, van den Bogert, Bennett, and Bull, Kotsifaki et al.(2022)Kotsifaki, Van Rossom, Whiteley, Korakakis, Bahr, Sideris, and Jonkers], [Arones et al.(2020)Arones, Shourijeh, Patten, and Fregly], and optimizing robotic design for individuals with impairments [Grabke et al.(2019)Grabke, Masani, and Andrysek]. Although physics-based models explicitly explain and map sEMG signals to joint kinematics, the high cost of their static optimization has always limited the practical applications of these models [Zhang et al.(2022a)Zhang, Zhao, Shone, Li, Frangi, Xie, and Zhang, Zhao et al.(2022a)Zhao, Zhang, Li, Qian, Xie, Lu, and Zhang].

Recently, deep neural networks (DNNs) provide an alternative solution to map the sEMG signals to the joint kinetics and kinematics [Dorschky et al.(2020)Dorschky, Nitschke, Martindale, Van den Bogert, Koelewijn, and Eskofier, Johnson et al.(2018)Johnson, Alderson, Lloyd, and Mian]. In this kind of model, the multi-layer convolution architecture has been explored to establish relationships between movement variables and neuromuscular status [Chaudhary et al.(2022)Chaudhary, Gerard, Wang, Christensen, Cooper, Schroeder, Hoffman, and Reinhardt, Zhang et al.(2022b)Zhang, Zhao, Bao, Li, Qian, Frangi, Xie, and Zhang]. For example, Nasr et al [Nasr et al.(2021)Nasr, Bell, He, Whittaker, Jiang, Dickerson, and McPhee] mapped the sEMG signals to the regression of joint angle, joint velocity, joint acceleration, joint torque, and activation torque, illustrating that the multi-layer convolution operators are capable of extracting underlying motor control information. Zhang et al [Zhang et al.(2022b)Zhang, Zhao, Bao, Li, Qian, Frangi, Xie, and Zhang] developed an active deep convolutional neural network to enhance the dynamic tracking capability of the musculoskeletal model on unseen data.

Despite the advantages, traditional DNNs are data-hungry and their performance is highly dependent on the quantity and quality of data [Solares et al.(2020)Solares, Raimondi, Zhu, Rahimian, Canoy, Tran, Gomes, Payberah, Zottoli, Nazarzadeh, et al.]. Meanwhile, biomechanics analysis is typically a physics-based extrapolation process with small sample nature [Shadlen et al.(1996)Shadlen, Britten, Newsome, and Movshon, Holder et al.(2020)Holder, Trinler, Meurer, and Stief]. Therefore, it is a challenge to train DNNs with small sample data so that the DNNs perform consistently with the physics-based model. To fill this research gap, the low-shot learning (LSL) technique has attracted many researchers' attention [Hu et al.(2022)Hu, Chapman, Wen, and Hall, Tam et al.(2022)Tam, Boukadoum, Campeau-Lecours, and Gosselin, Rahimian et al.(2021a)Rahimian, Zabihi, Asif, Atashzar, and Mohammadi]. For example, Rahimian *et al* [Rahimian et al.(2021b)Rahimian, Zabihi, Asif, Farina, Atashzar, and Mohammadi] introduced a Few-Shot Learning Hand Gesture Recognition (FS-HGR) model to enhance the generalization capability of DNNs from a limited number of instances. Lehmler *et al* [Lehmler et al.(2022)Lehmler, Saif-ur Rehman, Tobias, and Iossifidis] explored a low-shot learning methodology that adjusts DNNs to new users with only a small size of training data.

In addition, the generative adversarial network (GAN) framework has shown great potential in handling physical extrapolating and predictive problems [Goodfellow(2014), Goodfellow et al.(2020)Goodfellow, Pouget-Abadie, Mirza, Xu, Warde-Farley, Ozair, Courville, and Bengio, Chaudhary et al.(2022)Chaudhary, Gerard, Wang, Christensen, Cooper, Schroeder, Hoffman, and Reinhardt]. The GAN-based model is capable of discovering the structured patterns of the references and extrapolating the underlying data distribution characteristics during the adversarial learning process [Shi et al.(2022)Shi, Han, Han, Chang, Hu, and Dancey]. For example, Chen *et al* [Chen et al.(2022)Chen, Qian, Wang, and Fang] tested and evaluated the performance of the deep convolutional generative adversarial network (DCGAN) on sEMG-based data enhancement, and their results indicated that the extrapolated data is able to augment the diversity of the original data. Fahimi *et al* [Fahimi et al.(2020)Fahimi, Dosen, Ang, Mrachacz-Kersting, and Guan] proposed a generative adversarial learning framework for generating artificial electroencephalogram (EEG) data to extrapolate the brain-computer interface, and their findings suggest that generated EEG augmentation can significantly improve brain-computer interface performance.

In this study, we propose a physics-informed low-shot learning method for muscle force and joint kinematics estimation from multi-channel sEMG signals. This method seamlessly integrates physics knowledge with the GAN framework for structured feature decoding and extrapolated estimation from the small sample data. Specifically, Lagrange's equation of motion is introduced into the generative model to restrain the structured decoding of the high-level features following the laws of physics. And a physics-informed policy gradient is designed to improve the adversarial learning efficiency by rewarding the consistent physical representation of the extrapolated estimations and the physical references. Results show the muscle forces and joint kinematics estimated from the proposed method are unbiased compared to the physics-based inverse dynamics.

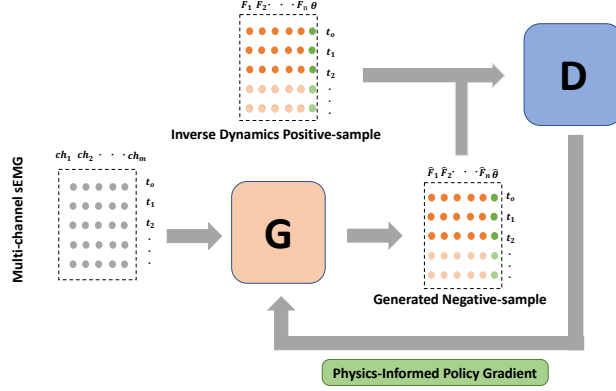


Figure 1: The main architecture of the proposed physics-informed low-shot generative adversarial learning for muscle force and joint kinematics prediction from multi-channel sEMG time-series

The remainder of this paper is organized as follows: Section 2 detailed describes the algorithm of the proposed physics-informed policy gradient for reinforcement generative adversarial learning, including the mathematics framework of the algorithm and network architectures. Section 3 presents the material and experimental methods. Section 4 discusses the experimental results and model evaluations. and Section 5 presents the conclusions.

## 2 Physics-informed low-shot learning method

The continuous estimation of muscle forces ( $F$ ) and joint kinematics( $\theta$ ) from multi-channel sEMG can be denoted as the time-series generation problem. Thus, given a real multi-channel sEMG time series, we train a  $\sigma$  parameterized generative network  $G_\sigma$  to estimate the muscle force ( $\hat{F}$ ) and joint kinematics ( $\hat{\theta}$ ). In this section, we propose a GAN framework, as shown in Fig.1, to train the  $G_\sigma$  on the small sample data. Specifically, we denote the  $\hat{F}$  and  $\hat{\theta}$  estimated by  $G_\sigma$  as the negative samples (see details in Section 2.2), the ground truth ( $\theta$ ) and the inverse dynamics-based ( $F$ ) [Zhao et al.(2022b)Zhao, Yu, Wang, Ma, Sheng, and Zhu] as positive samples (i.e. references). The  $\phi$ -parameterized discriminative model  $D_\phi$  is introduced to distinguish the positive samples and negative samples (see details in Section 2.3). During adversarial learning, the task of  $D_\phi$  is to determine if an input sample is positive or negative, and the task of  $G_\sigma$  is to generate the unbiased negative samples to fool the discriminator  $D_\phi$ . The model optimization process is driven by the newly proposed physics-informed policy gradient (see details in Section 2.1) which rewards the homogeneity of physics representation and structural characteristics between the positive and negative samples.

### 2.1 GAN optimization via physics-informed policy gradient

The physics-informed policy gradient method, inspired by reinforcement learning [Yu et al.(2017)Yu, Zhang, Wang, and Yu], aims to optimize the learning process of the GAN-based model yielding physical extrapolations from the small sample data (i.e. low-shot learning). Mathematically, the physics-informed policy gradient method maximizes its expected reward  $J(\sigma)$  based on the physics law and structured characteristics from the small sample data. The  $J(\sigma)$  consists of two parts, the structural reward  $R_{G_\sigma}$  and physics representation action  $Q_{D(\phi)}^{G(\sigma)}$ . The  $J(\sigma)$  is defined as follows.

$$\begin{aligned}
 J(\sigma) &= \mathbb{E}[R_{G_\sigma}(G_\sigma(sEMG_{0:T}))] \\
 &\quad \cdot Q_{D(\phi)}^{G(\sigma)}((G_\sigma(sEMG_{0:T}), [F, \theta]_{0:T})) \\
 &= \mathbb{E}[R_{G_\sigma}([\hat{F}, \hat{\theta}]_{0:T})] \\
 &\quad \cdot Q_{D(\phi)}^{G(\sigma)}([\hat{F}, \hat{\theta}]_{0:T}, [F, \theta]_{0:T})
 \end{aligned} \tag{1}$$

where  $sEMG_{0:T}$  is the input multi-channel sEMG time series for  $T$  time steps. The  $J(\sigma)$  is beginning with the expected reward from a predetermined state from the positive samples. And then, the  $R_{G_\sigma}$  and  $Q_{D(\phi)}^{G(\sigma)}$  will jointly optimize the generative network  $G_\sigma$  to generate the unbiased  $([\hat{F}, \hat{\theta}]_{0:T})$  following the physics laws.

Specifically, the structural reward  $R_{G_\sigma}$  is computed by the  $G_\sigma$  and defined as follows.

$$R_G([\hat{F}, \hat{\theta}]_{0:T}) = \exp^{PL^2([\hat{F}, \hat{\theta}]_{0:T})} \quad (2)$$

where  $PL([\hat{F}, \hat{\theta}]_{0:T})$  is the physics law used to restrict the hierarchical structure of the generated data, which provides the additional information to the regularize the learning process from the small sample data. In this case, we use the Lagrange equation of motion [Zhao et al.(2022b)Zhao, Yu, Wang, Ma, Sheng, and Zhu] as the physics law, which is defined as follows.

$$PL([\hat{F}, \hat{\theta}]_{0:T}) = \frac{1}{T} \sum_{t=1}^T (m(\hat{\theta}_t) \ddot{\hat{\theta}}_t + c(\hat{\theta}_t, \dot{\hat{\theta}}_t + g(\hat{\theta}_t) - \sum_{n=1}^N \hat{F}_t^n)^2) \quad (3)$$

where  $T$  is the number of time-steps,  $N$  is the channels of the  $\hat{F}$ ,  $m(\hat{\theta}_t)$ ,  $c(\hat{\theta}_t, \dot{\hat{\theta}}_t)$ , and  $g(\hat{\theta}_t)$  denote mass matrix, the Centrifugal and Coriolis force, and the gravity, respectively [Zhang et al.(2022a)Zhang, Zhao, Shone, Li, Frangi, Xie, and Zhang]. In this manner, the  $G_\sigma$  will generate the structured outputs of  $(\hat{F}, \hat{\theta})$ .

The  $Q_{D(\phi)}^{G(\sigma)}$  is computed by the  $D(\phi)$  and interprets the physics constraint action values as the estimated probability of being physics real by  $D(\phi)$ . These physics constraint action values lead to the improvement of GAN model in physical extrapolation from the small training data. The  $Q_{D(\phi)}^{G(\sigma)}$  can be formulated as:

$$Q_{D(\phi)}^{G(\sigma)}((G_\sigma(sEMG_{0:T}), [F, \theta]_{0:T}) = \mathbb{E}_{[\hat{F}, \hat{\theta}]_{0:T} \sim [F, \theta]_{0:T}} [\log D\phi([\hat{F}, \hat{\theta}]_{0:T})] + \mathbb{E}_{[\hat{F}, \hat{\theta}]_{0:T} \sim G_\sigma(sEMG_{0:T})} [\log(1 - D\phi([\hat{F}, \hat{\theta}]_{0:T}))] \quad (4)$$

For each epoch, once the new  $R_G$  and  $Q_{D(\phi)}^{G(\sigma)}$  has been obtained, the policy model  $G(\sigma)$  will be updated following the gradient of the reward function as follows.

$$\nabla_\sigma J(\sigma) = \mathbb{E}_{[\hat{F}, \hat{\theta}]_{0:T} \sim G_\sigma(sEMG_{0:T})} \sum \nabla_\sigma R_{G_\sigma}([\hat{F}, \hat{\theta}]_{0:T} | [F, \theta]_{0:T}) \cdot Q_{D(\phi)}^{G(\sigma)}([\hat{F}, \hat{\theta}]_{0:T}, [F, \theta]_{0:T}) \quad (5)$$

Using likelihood ratios, the unbiased estimation for Eq. 5 on one epoch can be described as follows.

$$\begin{aligned} \nabla_\sigma J(\sigma) &\simeq \frac{1}{T} \sum_{t=1}^T \sum_{y_t \in [\hat{F}, \hat{\theta}]_t} \nabla_\sigma R_{G_\sigma}(y_t | [F, \theta]_t) \cdot Q_{D(\phi)}^{G(\sigma)}(y_t, [F, \theta]_t) \\ &= \frac{1}{T} \sum_{t=1}^T \sum_{y_t \in [\hat{F}, \hat{\theta}]_t} G_\sigma(y_t | [F, \theta]_t) \nabla_\sigma \log G_\sigma(y_t | [F, \theta]_t) \\ &\quad \cdot Q_{D(\phi)}^{G(\sigma)}(y_t, [F, \theta]_t) \end{aligned} \quad (6)$$

The parameters of the policy model  $G_\sigma$  can be updated as follows.

$$\sigma \leftarrow \sigma + \alpha \nabla_\sigma J(\sigma) \quad (7)$$

where  $\alpha \in \mathbb{R}$  is the learning rate.

To summarize, Algorithm 1 provides an in-depth look at our proposed GAN optimization via a physics-informed policy gradient. Initially,  $G_\sigma$  is pre-trained on the training set  $sEMG = \{X_{1:T}\}$  using the maximum likelihood estimation (MLE). And then, the  $G_\sigma$  and  $D_\phi$  undergo adversarial learning. As the  $G_\sigma$  improves, the  $D_\phi$  is routinely retrained to stay synchronized with the  $G_\sigma$  improvement. We ensure balance by generating an equal number of negative samples for each training step as the positive samples.

**Algorithm 1** Generative adversarial learning via physics-informed policy gradient

---

**Require:** generator network  $G_\sigma$ ; discriminator  $D_\phi$ ; input multi-channel sEMG dataset  $sEMG = \{X_{1:T}\}$ ; Inverse dynamics positive samples  $Pos$

- 1: Initialize  $G_\sigma, D_\phi$  with random weights  $\sigma, \phi$ .
- 2: Pre-train  $G_\sigma$  using MLE on  $sEMG$
- 3:  $Pos \leftarrow G_\sigma$
- 4: Generate negative samples using  $G_\sigma$  for training  $D_\phi$
- 5: Pre-train  $D_\phi$  via minimizing the cross entropy
- 6: **repeat**
- 7:   **for**  $G_\sigma$  training-steps **do**
- 8:     Generate  $[\hat{F}, \hat{\theta}]$  time series via  $G_\sigma$
- 9:     **for**  $t$  in  $0:T$  **do**
- 10:       Compute  $Q_{D_\phi}^{G_\sigma}$  by Eq. 4
- 11:     **end for**
- 12:     Update generator parameters via physics-informed reward Eq. 7
- 13:   **end for**
- 14:   **for** d-steps **do**
- 15:     Use current  $G_\sigma$  to generate negative examples and combine them with given positive examples  $Pos$
- 16:     Train discriminator  $D_\phi$  for  $k$  epochs.
- 17:   **end for**
- 18:    $\beta \leftarrow \sigma$
- 19: **until** GAN converges

---

## 2.2 The generative network

The proposed physics-informed low-shot learning method does not depend on the specific generative network architecture. In this study, considering the long-term temporal dependencies of the  $F$  and  $\theta$  sequences to the input multi-channel sEMG sequence, we employ the Long Short-Term Memory (LSTM) cells to our generative model [Han et al.(2019)Han, Zhou, Geng, Chen, Wang, and Wei]. The architecture of the generator network  $G$  is shown in Fig.2. It serves three functions: multi-channel sEMG feature extraction, residual learning with LSTM, and musculoskeletal tokens sequence generation.

Firstly, for the multi-channel sEMG feature extraction, a 1-dimensional (1D) convolution filter with a  $2/times1$  kernel is introduced to capture the multiple sEMG features at time step  $t$ . The extracted convolution features represent the hierarchical structures of the multi-channel sEMG. In this study, the convolution kernel is set to  $1 \times b$  for a  $b$ -channel sEMG input. Considering the batch normalization (BN) layer would normalize the features and get rid of the range flexibility for upscaling features [Nah et al.(2017)Nah, Hyun Kim, and Mu Lee], no BN layer is used here to avoid blurring the sEMG responses hidden in the extracted features. The max-pooling layer is used to combine the extracted sEMG features into a single neuron by using the maximum value from each convolution window. The max-pooling operation reduces the number of parameters and network computation costs and has the effect of adjusting over-fitting.

Secondly, the LSTM blocks are employed for residual learning of the time-series characteristics of the target musculoskeletal tokens. The LSTM layer is well suited for time-series sequence generation by addressing the explosive and vanishing gradient issues [Yu et al.(2017)Yu, Zhang, Wang, and Yu]. An LSTM block consists of a memory cell, an input gate, an output gate, and a forget gate, the detailed definitions of the components are described in [Nah et al.(2017)Nah, Hyun Kim, and Mu Lee]’s study. Specifically, in this study, in time step  $t$ , the memory cell remembers structured feature values over the previous  $t - 1$  intervals and the three gates regulate the flow of information into and out of the memory cell, which has a great preference for preserving long-term temporal structure characteristics by consolidating previous temporal correlations as memory units. Meanwhile, the high-level sEMG features extracted from the convolution layer represent the current multi-channel sEMG responses to muscle force and joint kinematics. The skip-connect of the memory cell and the high-level sEMG features not only represent extracted local kinetic invariances but also represent the temporal dynamics of the motions.

It is noteworthy that the traditional LSTM layer only produces fitness between the current time step and the previous time steps. However, we expect the model also can pay insight into the resulting future outputs. In order to compute the action value for future physical fitness, a Monte Carlo (MC) search with a roll-out strategy is used to sample the unknown last  $T - t$  time steps. and the  $N$ -time Monte Carlo search can be formulated as:

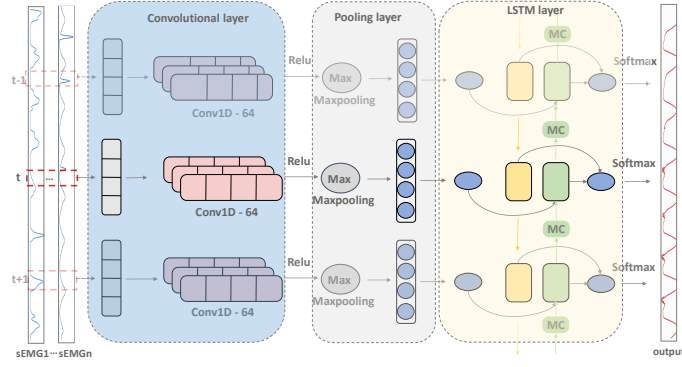


Figure 2: The network architecture of the generator network in the proposed physics-informed reinforcement generative adversarial learning.

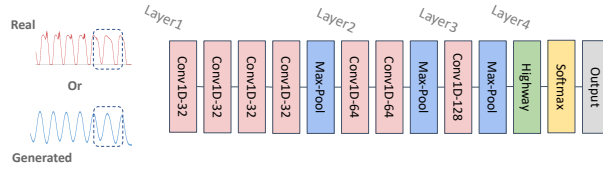


Figure 3: The network architecture of the discriminative model in the proposed physics-informed reinforcement generative adversarial learning.

$$\{(F_{0:T}, \theta_{0:T})^1, \dots, (F_{0:T}, \theta_{0:T})^N = MC(F_{0:t}, \theta_{0:t})\} \quad (8)$$

Finally, the fully connected layers are used to generate the musculoskeletal tokens sequence over a motion period. The output of the LSTM unit is flattened to a feature vector and scaled to the muscle force  $F$  and joint kinematics  $\theta$ .

### 2.3 The discriminative model

In this study, a  $\phi$  parameterized discriminator network  $D_\phi$  is built to guide the iterations of  $G_\sigma$  from the small sample data.  $D_\phi$  outputs a probability indicating the heterogeneity between  $[\hat{F}, \hat{\theta}]$  and  $[F, \theta]$ . For this purpose, we employ a convolution neural network (CNN) [Wu et al.(2020)Wu, Liu, and Wang] as the discriminative model because of its successful applications in sequence classification. In this study, we concentrate on the situation where the discriminator estimates the likelihood of a completed  $[\hat{F}, \hat{\theta}]$  time-series from the physical-law model (i.e.  $ID$ ).

We first represent an input muscle force and joint kinematics time series  $x_1, \dots, x_T$  as

$$E_{0:T} = [\hat{F}, \hat{\theta}]_0 \oplus [\hat{F}, \hat{\theta}]_1 \oplus \dots \oplus [\hat{F}, \hat{\theta}]_T \quad (9)$$

where,  $x_t \in \mathbb{R}^b$  is the muscle force and joint kinematics in time-step  $t$  and  $\oplus$  is the concatenation operator to build the matrix  $E_{1:T} \in \mathbb{R}^T$ . Then the convolution operator is used to produce a new feature map:

$$c_i = \rho(w \odot E_{i:i+l-1} + b) \quad (10)$$

where  $\odot$  is the element-wise production,  $b$  is a bias term and  $\rho$  is a non-linear function. In this study, the discriminator, as shown in Fig.3, employs various numbers of kernels with different window sizes to extract different features from the input musculoskeletal sequence. And the max-pooling operation over the feature maps to reduce the number of parameters and network computation costs. In order to enhance the discrimination performance, a highway operator [Srivastava et al.(2015)Srivastava, Greff, and Schmidhuber] based on the pooled feature maps is also employed in our discriminative model. Finally, a fully connected layer with softmax activation is used to output the estimation of the likelihood that the input sequence conforms to physical laws.

### 3 MATERIAL AND EXPERIMENTAL METHODS

In this study, we test our proposed method on two joint motion scenarios. The first one is the knee joint modeling from an open-access dataset of walking trials, and the second one is the wrist joint modeling from the self-collected dataset of wrist motions.

#### 3.1 Open-access dataset of walking trials

The open-access dataset of walking trails is obtained from a real-world experiment reported in [Liu et al.(2008)Liu, Anderson, Schwartz, and Delp]. This dataset involves six healthy participants with an average age of  $12.9 \pm 3.2$  years and an average weight of  $51.8 \pm 19.1$  Kg. Participants are instructed to walk at four distinct speeds, which include very slow ( $0.53 \pm 0.1$  m/s), slow ( $0.75 \pm 0.1$  m/s), free ( $1.15 \pm 0.08$  m/s), and fast ( $1.56 \pm 0.21$  m/s) speeds. The sEMG signals are captured from the *biceps femorisshorthead* (BFS) and the *rectus femoris* (RF) as they are the primary flexor and extensor of the knee joint. In this study, we normalize each gait cycle into 100 frames for model training and testing, and the original data for model extrapolation evaluation. In the model training and testing session, each walking trial sample is formatted into a source matrix that includes the time step, gait motion data, and enveloped sEMG signals. All of the samples from different participants are combined to create a comprehensive dataset for model training and testing.

#### 3.2 Self-collected dataset of wrist motions

Our wrist motions experiment, approved by the MaPS and Engineering Joint Faculty Research Ethics Committee of the University of Leeds (MEEC 18-002), involved six participants with signed consent. Participants were instructed to keep their torso straight with their shoulder abducted at 90 degrees and their elbow joint flexed at 90 degrees. The VICON motion capture system is used to record continuous wrist flexion/extension motion. Joint motions are calculated using an upper limb model with 16 reflective markers with 250 Hz sampling rate. Concurrently, sEMG signals are captured from the primary wrist muscles ( $n = 1, 2, \dots, 5$ ), including the *flexorcarpiradialis* (FCR), the *flexorcarpiulnaris* (FCU), the *extensorcarpiradialislongus* (ECRL), the *extensorcarpiradialisbrevis* (ECRB), and the *extensorcarpiulnaris* (ECU) using Avanti Sensors (sampling rate is 2000 Hz). Electrodes are placed by palpation and their placement is validated by observing the signal during contraction before the experiment. The sEMG signals and motion data were synchronized and resampled at 1000 Hz. Each participant performed five repetitive trials with a three-minute break between trials to prevent muscle fatigue.

The recorded sEMG signals are pre-processed by a 20 Hz and 450 Hz band-pass filter, full rectification, and a 6 Hz low-pass filter. These signals are then normalized based on the maximum voluntary contraction recorded prior to the experiment, yielding the enveloped sEMG signals. We normalize each motion cycle into 156 frames for model training and testing, and the original data for model extrapolation evaluation. A total of 360 motion data are then combined to create a comprehensive dataset for model training and testing, and 6 motion data are used for model evaluation.

#### 3.3 Benchmark models and parameter settings

To evaluate the performance and effectiveness of the proposed physics-informed policy gradient for low-shot generative adversarial learning, the benchmark models employ three representative methods, including physics-Informed convolutional neural network (PI-CNN) [Zhang et al.(2022a)Zhang, Zhao, Shone, Li, Frangi, Xie, and Zhang] which represents the state-of-the-art deep learning based musculoskeletal modeling method, ML-ELM [Zhang et al.(2016)Zhang, Ding, and Zhang] which represents the general musculoskeletal modeling method, and the vanilla GAN which represents the traditional GAN family without physical-law [Goodfellow(2014)].

#### 3.4 Evaluation metrics

The evaluation metrics include 1) the metrics for evaluating the quality of the generated samples including the information entropy associated peak signal-to-noise ratio (PSNR) [Solnik et al.(2008)Solnik, DeVita, Rider, Long, and Hortobágyi], coefficient of Determination ( $R^2$ ) [Kahl and Hofmann(2016)], root mean square error (RMSE) [Zhao et al.(2022a)Zhao, Zhang, Li, Qian, Xie, Lu, and Zhang], Spearman’s Rank Correlation Coefficient (SRCC) [Pan et al.(2022)Pan, Liu, and Li], and 2) the metrics for evaluating the mode collapse of GANs, including 1) inception score (IS) [Shi et al.(2022)Shi, Han, Han, Chang, Hu, and Dancey], and 2) Frechet inception distance (FID) [Jung and Keuper(2021)].

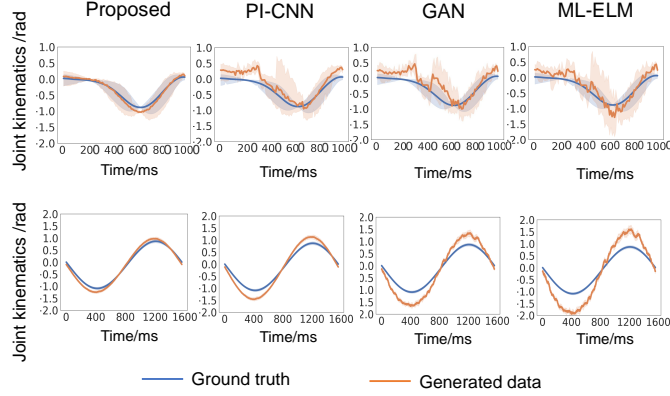


Figure 4: Comparison of the average knee joint kinematics (the first row) and wrist joint kinematics (the second row) within one gait cycle between the ground truth and the generated data from the proposed and benchmark models. The shaded areas represent the mean  $\pm$  one standard deviation of the kinematics.

## 4 Results and discussion

In this section, we evaluate the performance of the proposed physics-informed low-shot learning in the knee joint and wrist joint scenarios. We first carry out overall comparisons of the results from the proposed and benchmark methods. We also evaluate the model performance on small training data and handling mode collapse. Lastly, we investigate the robustness and generalization performance of the proposed method in intersession scenarios. The training of the proposed framework and benchmark methods was conducted using PyTorch on a workstation equipped with NVIDIA Quadro K4200 graphics cards and 256G RAM.

### 4.1 Overall evaluation of the muscle force dynamics modeling

In this section, we first carry out overall comparisons between the proposed and benchmark methods on the test dataset. Fig. 4 demonstrates the overall results of the joint kinematics generation in one motion circle from the proposed and benchmark methods for both the knee joint (the first row of Fig. 4) and wrist joint cases (the second row of Fig. 4). The average joint kinematics and standard deviation distribution from the proposed method align well with the ground truth in both the knee joint and wrist joint cases. These findings indicate the proposed model achieves the best performance among the benchmark models on the unbiased estimation of the joint kinematics.

Similarly, Fig. 5 and Fig.6 demonstrate the overall results of the muscle force estimations in one motion circle for both the knee joint (i.e. RF and BFS) and wrist joint (i.e. FCR, FCU, ECRL, ECRB, and ECU) cases, respectively. The average muscle forces estimated by the proposed method align well with the inverse dynamics, demonstrating the excellent multiple muscle tracking capability of the proposed model. In addition, the standard deviation distribution of the proposed model-generated muscle forces is perfectly consistent with the standard deviation distribution of the inverse dynamics-based references. These results indicate that the proposed model achieves the best performance among the benchmark models on the unbiased estimation of the muscle force from the multi-channel sEMG signals.

To further assess the extrapolation performance quantitatively, we present detailed comparisons of the proposed and benchmark models on both of the test data and evaluation data. Table 1 and Table 2 respectively shows the results for the knee joint case and the wrist joint case. The results indicate that the proposed model performs best on both of the testing and evaluation data. Specifically, for model testing, the  $PSNR$ ,  $R^2$ ,  $RMSE$ ,  $SRCC$  of the proposed model are 15.57%, 6.22%, 28.08%, 7.2% higher than that of the second best model (i.e. PI-CNN). For model evaluation, the  $PSNR$ ,  $R^2$ ,  $RMSE$ ,  $SRCC$  of the proposed model are 24.72%, 16.29%, 38.99%, 17.66% higher than that of the second best model (i.e. GAN). In addition, because the evaluation data involve the original sEMG recordings, the comparison of the testing results and evaluation results indicates the model extrapolation from the experimental scenarios to real scenarios. The proposed model shows the best extrapolated estimation of muscle force and joint kinematics among the benchmark models, the results from the testing data and evaluation data is consistent. In contrast, the performance of the benchmark models show serious decline on evaluation data.



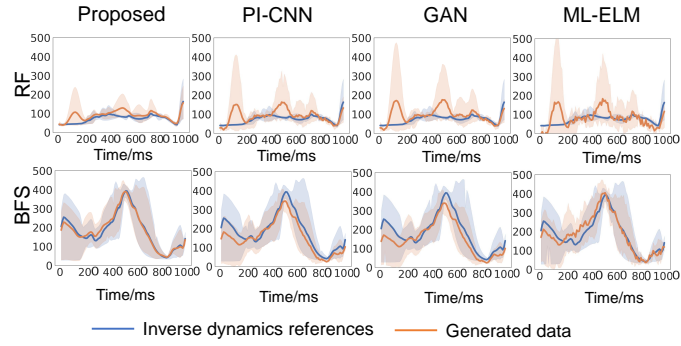


Figure 5: Comparison of the average knee muscle force dynamics within one gait cycle between the real-target and the generated muscle force data from the proposed and benchmark models. The shaded areas represent the mean  $\pm$  one standard deviation of the muscle force for BFS and RF.

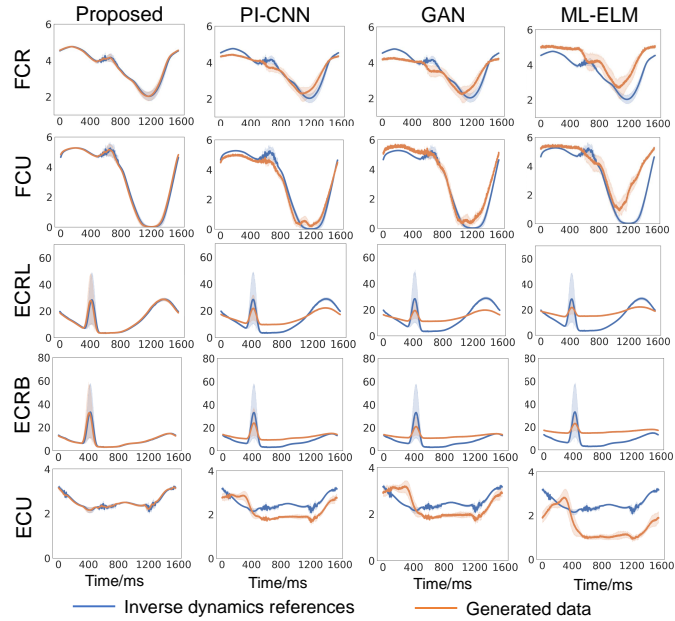


Figure 6: Comparison of the average wrist muscle force dynamics within one motion cycle between the real-target and the generated muscle force data from 5-channel sEMG signal. The shaded areas represent the mean  $\pm$  one standard deviation of the muscle force for FCR, FCU, ECRL, ECRB, and ECU.

Table 1: The evaluation of the proposed and benchmark models on knee joint case with two-channels sEMG.

		Model test			
	Methods	PSNR	R2	RMSE	SRCC
RF	Proposed	91.91	0.88	11.32	0.92
	PI-CNN	77.45	0.84	19.64	0.85
	GAN	75.54	0.82	18.25	0.81
	ML-ELM	59.94	0.76	25.62	0.72
BFS	Proposed	93.45	0.93	11.93	0.93
	PI-CNN	76.93	0.87	19.21	0.83
	GAN	76.17	0.85	18.35	0.79
	ML-ELM	62.66	0.78	26.43	0.73
$\theta$	Proposed	34.79	0.91	5.73	0.92
	PI-CNN	30.16	0.84	5.97	0.89
	GAN	30.89	0.88	6.57	0.85
	ML-ELM	21.33	0.75	11.25	0.73
		Model evaluation			
RF	Proposed	88.89	0.82	11.21	0.83
	PI-CNN	58.91	0.59	24.17	0.6
	GAN	68.72	0.7	26.51	0.69
	ML-ELM	46.79	0.53	28.75	0.5
BFS	Proposed	91.84	0.91	11.91	0.84
	PI-CNN	58.19	0.61	23.58	0.58
	GAN	69.26	0.72	25.79	0.67
	ML-ELM	49.21	0.55	38.98	0.51
$\theta$	Proposed	34.89	0.92	5.45	0.91
	PI-CNN	23.43	0.59	8.3	0.62
	GAN	28.27	0.75	7.89	0.72
	ML-ELM	17.19	0.53	18.44	0.51

Table 2: The evaluation of the proposed and benchmark models on wrist joint case with five-channels sEMG

		Model test									
	Methods	PSNR	R2	RMSE	SRCC		Methods	PSNR	R2	RMSE	SRCC
FCR	Proposed	31.91	0.92	5.32	0.94	FCU	Proposed	33.61	0.93	4.37	0.96
	PI-CNN	27.45	0.84	9.64	0.83		PI-CNN	29.01	0.86	10.43	0.83
	GAN	25.54	0.86	8.25	0.81		GAN	25.27	0.88	8.6	0.79
	ML-ELM	19.94	0.74	15.62	0.72		ML-ELM	18.42	0.76	14.95	0.73
ECRL	Proposed	84.21	0.95	14.68	0.94	ECRB	Proposed	82.93	0.95	14.78	0.97
	PI-CNN	79.4	0.84	25.08	0.83		PI-CNN	79.75	0.88	24.32	0.81
	GAN	61.54	0.9	24.55	0.82		GAN	59.71	0.91	24.62	0.79
	ML-ELM	57.76	0.77	42.41	0.76		ML-ELM	57.4	0.78	41.82	0.77
ECU	Proposed	30.81	0.92	5.14	0.92	theta	Proposed	34.32	0.97	3.75	0.96
	PI-CNN	30.31	0.84	10.06	0.82		PI-CNN	29.94	0.84	4.63	0.88
	GAN	28.06	0.87	7.92	0.8		GAN	30.34	0.86	4.51	0.85
	ML-ELM	19.85	0.75	14.72	0.71		ML-ELM	21.15	0.76	9.62	0.74
		Model evaluation									
FCR	Proposed	29.96	0.87	5.05	0.89	FCU	Proposed	31.35	0.88	4.15	0.91
	PI-CNN	20.49	0.63	10.23	0.62		PI-CNN	21.75	0.65	9.82	0.62
	GAN	22.43	0.77	11.43	0.73		GAN	21.8	0.79	12.74	0.71
	ML-ELM	14.09	0.56	19.72	0.54		ML-ELM	13.57	0.57	21.21	0.55
ECRL	Proposed	79.76	0.9	13.95	0.89	ECRB	Proposed	78.33	0.9	14.04	0.92
	PI-CNN	58.65	0.63	28.81	0.62		PI-CNN	59.81	0.66	28.24	0.61
	GAN	54.52	0.81	32.1	0.74		GAN	53.7	0.82	24.11	0.71
	ML-ELM	42.45	0.58	39.81	0.57		ML-ELM	42.3	0.59	51.37	0.58
ECU	Proposed	28.64	0.87	4.88	0.87	theta	Proposed	31.75	0.92	3.56	0.91
	PI-CNN	22.29	0.63	10.55	0.62		PI-CNN	21.73	0.63	6.47	0.66
	GAN	24.41	0.78	11.13	0.72		GAN	25.58	0.77	8.06	0.77
	ML-ELM	14.28	0.56	16.04	0.53		ML-ELM	15.43	0.57	11.22	0.56

## 4.2 Evaluation of low-shot learning

The proposed physics-informed policy gradient incorporates the temporal relationship of the muscle force and joint kinematics dynamics from the Lagrange motion equation, resulting in an improved kinetics estimation from the low-shot samples. Initially, the physical information is used to constrain the model reward accumulated following the periodic multi-channel sEMG signals. And then, the accumulative reward is used to guide the Monte Carlo search to generate the unbiased estimation of muscle force and joint kinematics dynamics.

To quantitatively assess the effectiveness of the proposed method on low-shot learning, we firstly regard the modeling results shown in Table 1 and Table 2 as the baselines that represent the optimal performance of the proposed and benchmark models, and then we train the models with different training sample sizes for 1500 epochs as low-shot learning. The percentages of the low-shot learning results and the baseline joint kinematics modeling results, denote as  $P - PSNR$ ,  $P - R^2$ ,  $P - RMSE$ , and  $P - SRCC$ , are used as the evaluation metrics to describe what percentage of the performance of the baseline models can be achieved with the new models.

The evaluation of the low-shot learning of the proposed and benchmark models on the knee joint and wrist joint kinematics modeling is shown in Table 3. It is obvious that the proposed model with a physics-informed policy gradient outperforms all of the benchmark models in low-shot learning. The 10-shot learning is able to achieve over 80% baseline performance in terms of  $PSNR$ ,  $R^2$ ,  $RMSE$ , and  $SRCC$ . In comparison, the PINN and GAN models achieving a similar modeling performance require at least 80-shot learning. Therefore, it can be inferred that the proposed physics-informed policy gradient relies heavily on the physical representations and temporal structural characteristics of the training data, rather than the quantity of the data. This is encouraging as it suggests that the proposed method facilitates the applications of deep learning in biomechanical engineering from the general issue of limited sample size.

## 4.3 Mode collapse evaluation

Mathematically, the generative model is easy to find a biased estimation caused by mode collapse, which leads to the generated samples only being located in the partial real distribution where it can fool the discriminative model and ignore other modes of real distribution during the adversarial learning. To handle this issue, the proposed physics-informed policy gradient alleviates the random noises and makes the generated feature sequence governed by the physics law, which facilitates the estimation of compound kinematics patterns and achieves the unbiased estimation of kinematics generation.

In order to evaluate the performance of the proposed method on alleviating the mode collapse, we test and compare the proposed model with the benchmark model from two aspects: 1) a quantitative evaluation of the diversity of the generated motions, based on the distance-derived IS and FID metrics; and 2) a monotonicity assessment on the generator iterations during the network training process; and 3) visualization of the distributions of the real and the generated motion samples. Firstly, the quantitative evaluation for the diversity of the generated motions is conducted on the testing dataset. The higher IS and lower FID indicate the better diversity of the generated super-resolution HSIs, which further indicates the alleviation of mode collapse.

The results demonstrated in Table 4 show the proposed model outperforms the competitors in terms of the IS and FID measurements for both the knee joint and wrist joint motion generation. In addition, the benchmark GAN model, with the network architecture as same as the proposed model, is 19.11% higher in IS, and 14.23% lower in FID than the proposed model. These findings suggest that the proposed physics-informed policy gradient optimization approach has great performance in alleviating the mode collapse during adversarial learning.

Secondly, in order to further explore the performance of the proposed physics-informed policy gradient on the mode collapse issue, we compare the generator iterations of the same GAN architectures with and without the physics-informed policy gradient (Fig. 7). The IS and FID curves from the GAN with the proposed physics-informed policy gradient are more monotonous than the GAN without the physics-informed policy gradient, along with the increase of iteration number. Thus, the curves of IS from the proposed physics-informed policy gradient steadily increase and the curves of FID steadily decrease for both knee joint (7a and b) and wrist joint (7c and d) cases.

## 4.4 Model application on intra-session scenario

In musculoskeletal modeling, the intra-session scenario is regarded as the multiple sets of motions that occur within the same session. To test the robustness of the proposed model in the intra-session scenario, we use the knee joint data with different walking speeds for one subject as the intra-session evaluation dataset. The muscle force and joint kinematics modeling results, as shown in Fig. 8, indicate that the proposed framework performs best among the baseline methods. Importantly, the median and interquartile values of the proposed model with physics-informed policy gradient remain consistent with the real data across different walking speeds. In comparison, the median and quartiles of the baseline

Table 3: Evaluation of the low-shot learning performance of the proposed and benchmark models on joint kinematics modeling. The  $P - PSNR$ ,  $P - R^2$ ,  $P - RMSE$ , and  $P - SRCC$  respectively represent the  $SNR$ ,  $R^2$ ,  $RMSE$ , and  $SRCC$  of the  $n$ -shot learning as a percentage of the validation metrics of the best joint kinematics results report in Table.1 and Table 2.

		Knee joint case				Wrist joint case			
		P-PNSR	P- $R^2$	P-RMSE	P-SRCC	P-PNSR	P- $R^2$	P-RMSE	P-SRCC
Proposed	1-shot	75%	74%	76%	75%	76%	73%	77%	75%
	10-shot	83%	82%	84%	87%	82%	81%	84%	88%
	20-shot	86%	84%	86%	86%	87%	86%	88%	84%
	40-shot	92%	91%	92%	91%	93%	91%	93%	94%
	60-shot	94%	94%	92%	94%	96%	97%	93%	93%
	80-shot	93%	94%	95%	94%	92%	93%	97%	94%
	100-shot	95%	94%	93%	93%	96%	94%	93%	96%
		P-PNSR	P- $R^2$	P-RMSE	P-SRCC	P-PNSR	P- $R^2$	P-RMSE	P-SRCC
PINN	1-shot	41%	41%	41%	39%	42%	42%	44%	39%
	10-shot	44%	42%	44%	44%	46%	42%	45%	47%
	20-shot	68%	69%	72%	73%	69%	70%	72%	76%
	40-shot	76%	76%	77%	79%	77%	78%	8%	78%
	60-shot	79%	77%	76%	75%	78%	77%	76%	76%
	80-shot	82%	83%	84%	85%	81%	86%	83%	84%
	100-shot	84%	87%	85%	87%	85%	88%	85%	86%
		P-PNSR	P- $R^2$	P-RMSE	P-SRCC	P-PNSR	P- $R^2$	P-RMSE	P-SRCC
GAN	1-shot	46%	44%	47%	49%	45%	45%	48%	51%
	10-shot	45%	45%	45%	47%	48%	46%	44%	48%
	20-shot	66%	69%	7%	73%	67%	71%	70%	73%
	40-shot	72%	73%	74%	74%	74%	72%	72%	76%
	60-shot	79%	78%	81%	81%	78%	78%	80%	8%
	80-shot	81%	83%	85%	85%	79%	83%	86%	84%
	100-shot	84%	86%	87%	89%	86%	87%	86%	91%
		P-PNSR	P- $R^2$	P-RMSE	P-SRCC	P-PNSR	P- $R^2$	P-RMSE	P-SRCC
ML-ELM	1-shot	36%	35%	37%	38%	34%	37%	36%	37%
	10-shot	38%	44%	45%	39%	39%	39%	42%	38%
	20-shot	57%	56%	55%	54%	59%	56%	57%	55%
	40-shot	62%	62%	65%	59%	65%	61%	68%	58%
	60-shot	66%	65%	67%	66%	65%	64%	66%	67%
	80-shot	75%	73%	72%	74%	77%	74%	71%	74%
	100-shot	78%	79%	78%	81%	78%	82%	81%	82%

Table 4: The Comparison of Inception Scores (IS) and Frechet Inception Distances (FID) of the joint kinematics generated from the proposed and benchmark models on the model test datasets.

	Knee joint case		Wrist joint case	
	IS	FID	IS	FID
Proposed	10.59	79.83	6.79	57.05
PINN	13.11	78.54	8.43	46.13
GAN	12.68	71.13	8.03	48.8
ML-ELM	15.39	74.42	12.5	41.95

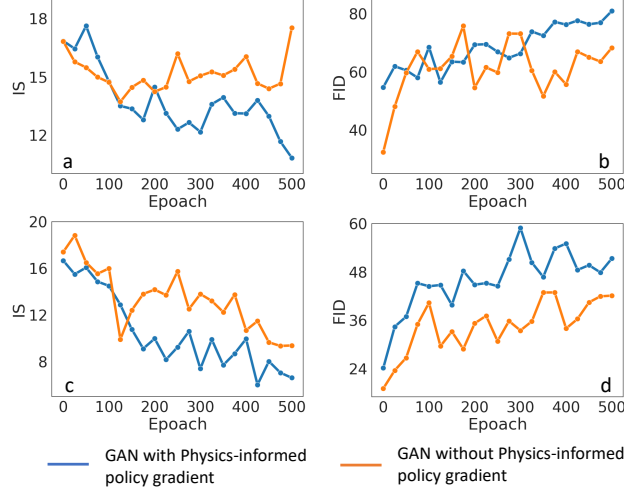


Figure 7: Changes of IS and FID scores of the generated joint kinematics during the first 500 iterations of the GAN model using the proposed physics-informed policy gradient and the typical GAN without using the physics-informed policy gradient. The test is conducted on knee joint cases (a) and (b) and wrist joint cases (c) and (d), respectively.

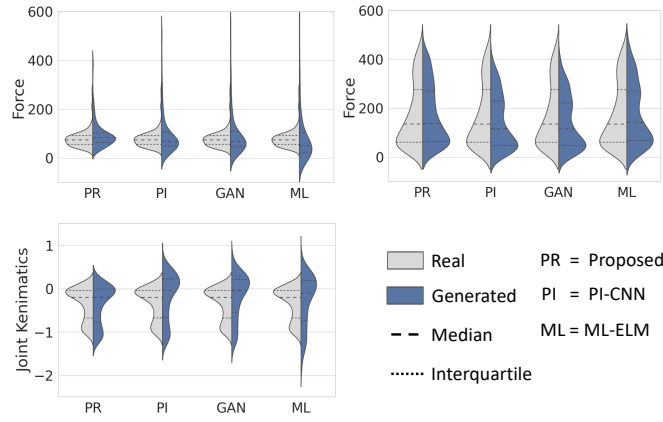


Figure 8: Robustness evaluation of the proposed model (PR), PI-CNN (PI), GAN, and ML-ELM (ML) on the intra-session scenario.

methods, such as the GAN model without using the physics-informed policy gradient, show significant inconsistencies with the real data, indicating a declined performance in the intra-session scenario due to the variability in walking speeds. These findings suggest that the model optimized by the proposed physics-informed policy gradient has great robustness in intra-session scenarios.

#### 4.5 Model application on inter-session scenario

The inter-session scenario generally refers to a situation where motion data are collected across multiple sessions. To test the robustness of the proposed model in the inter-session scenario, we use the wrist joint data with different subjects as the evaluation dataset. The muscle force and joint kinematics modeling results, as shown in Fig. 9, indicate that the proposed framework performs best on the musculoskeletal modeling among the baseline methods. Specifically, the median and interquartile values of the proposed model with physics-informed policy gradient remain consistent with the real data across different subjects. In comparison, the baseline methods, such as the GAN model without using the physics-informed policy gradient, show a declined performance in the inter-session scenario due to the variability in walking speeds. These findings suggest that the model optimized by the proposed physics-informed policy gradient has great robustness in inter-session scenarios.

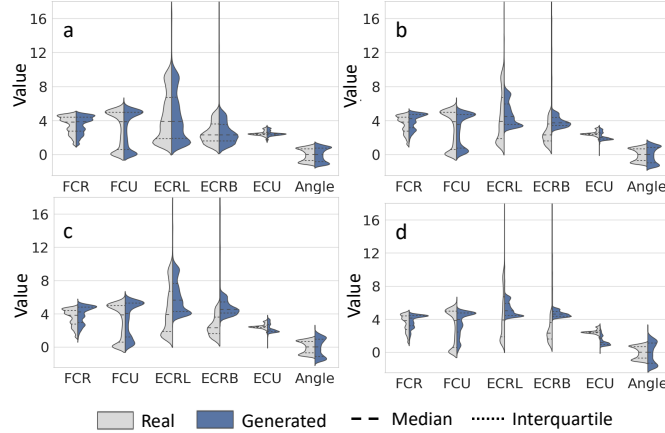


Figure 9: Robustness evaluation of the a) proposed model, b) PI-CNN, c) GAN, and d) ML-ELM (ML) on the inter-session scenario.

## 5 Conclusion

This paper develops a physics-informed low-shot learning method, which seamlessly integrates the Lagrange equation of motion and inverse dynamic muscle model into the adversarial learning process, to train the generative network for the unbiased estimation of the muscle force and joint kinematics from the small size sEMG time series. Specifically, the Lagrange equation of motion is introduced as physical constraint, which facilitates the generator to estimate the muscle force and joint kinematics with more temporal structural representations. Meanwhile, the physics-informed policy gradient rewards the physical consistency of the generated muscle force and joint kinematics and the inverse dynamics-based references, which improve the extrapolation performance of the generative network. Comprehensive experiments on the knee joints and wrist joints indicate the feasibility of the proposed method. The resultant findings suggest that the proposed method performs well in handling the mode collapse issue on the small sample data, and the estimations of the muscle forces and joint kinematics are unbiased compared to the physics-based inverse dynamics. These findings suggest that the proposed method may reduce the gaps between laboratory prototypes and clinical applications. However, it is worth noting that the physics reference (i.e. the inverse dynamics for this study) plays an important role in constraining the physics representation of the generated samples. Therefore, the choice of physics module may vary when the proposed approach is extended to other application cases.

Going forward, we plan to delve deeper into the properties of the physics-informed deep learning framework in the context of sEMG-based musculoskeletal modeling. We aim to investigate the potential of the low-shot learning-based model on the continuous and simultaneous estimation of multiple joint kinematic chains from sEMG signals. We also plan to adjust the compositions of the proposed method to cater to different application scenarios. Furthermore, we intend to evaluate the reliability and accuracy of the proposed framework through more complex movements.

## References

- [Falisse et al.(2019)Falisse, Serrancolí, Dembia, Gillis, Jonkers, and De Groote] Antoine Falisse, Gil Serrancolí, Christopher L Dembia, Joris Gillis, Ilse Jonkers, and Friedl De Groote. Rapid predictive simulations with complex musculoskeletal models suggest that diverse healthy and pathological human gaits can emerge from similar control strategies. *Journal of The Royal Society Interface*, 16(157):20190402, 2019.
- [Modenese and Kohout(2020)] Luca Modenese and Josef Kohout. Automated generation of three-dimensional complex muscle geometries for use in personalised musculoskeletal models. *Annals of Biomedical Engineering*, 48(6): 1793–1804, 2020.
- [Smith et al.(2021)Smith, Coppack, van den Bogert, Bennett, and Bull] Samuel HL Smith, Russell J Coppack, Antonie J van den Bogert, Alexander N Bennett, and Anthony MJ Bull. Review of musculoskeletal modelling in a clinical setting: Current use in rehabilitation design, surgical decision making and healthcare interventions. *Clinical Biomechanics*, 83:105292, 2021.
- [Kotsifaki et al.(2022)Kotsifaki, Van Rossom, Whiteley, Korakakis, Bahr, Sideris, and Jonkers] Argyro Kotsifaki, Sam Van Rossom, Rod Whiteley, Vasileios Korakakis, Roald Bahr, Vasileios Sideris, and Ilse Jonkers. Single

- leg vertical jump performance identifies knee function deficits at return to sport after acl reconstruction in male athletes. *British journal of sports medicine*, 56(9):490–498, 2022.
- [Arones et al.(2020)Arones, Shourijeh, Patten, and Fregly] Marleny M Arones, Mohammad S Shourijeh, Carolyn Patten, and Benjamin J Fregly. Musculoskeletal model personalization affects metabolic cost estimates for walking. *Frontiers in Bioengineering and Biotechnology*, 8:588925, 2020.
- [Grabke et al.(2019)Grabke, Masani, and Andrysek] Emerson Paul Grabke, Kei Masani, and Jan Andrysek. Lower limb assistive device design optimization using musculoskeletal modeling: a review. *Journal of Medical Devices*, 13(4), 2019.
- [Zhang et al.(2022a)Zhang, Zhao, Shone, Li, Frangi, Xie, and Zhang] Jie Zhang, Yihui Zhao, Fergus Shone, Zhenhong Li, Alejandro F Frangi, Sheng Quan Xie, and Zhi-Qiang Zhang. Physics-informed deep learning for musculoskeletal modelling: Predicting muscle forces and joint kinematics from surface emg. *IEEE Transactions on Neural Systems and Rehabilitation Engineering*, 2022a.
- [Zhao et al.(2022a)Zhao, Zhang, Li, Qian, Xie, Lu, and Zhang] Yihui Zhao, Jie Zhang, Zhenhong Li, Kun Qian, Sheng Quan Xie, Yu Lu, and Zhi-Qiang Zhang. Computational efficient personalised emg-driven musculoskeletal model of wrist joint. *IEEE Transactions on Instrumentation and Measurement*, 2022a.
- [Dorschky et al.(2020)Dorschky, Nitschke, Martindale, Van den Bogert, Koelewijn, and Eskofier] Eva Dorschky, Marlies Nitschke, Christine F Martindale, Antonie J Van den Bogert, Anne D Koelewijn, and Bjoern M Eskofier. Cnn-based estimation of sagittal plane walking and running biomechanics from measured and simulated inertial sensor data. *Frontiers in bioengineering and biotechnology*, 8:604, 2020.
- [Johnson et al.(2018)Johnson, Alderson, Lloyd, and Mian] William Robert Johnson, Jacqueline Alderson, David Lloyd, and Ajmal Mian. Predicting athlete ground reaction forces and moments from spatio-temporal driven cnn models. *IEEE Transactions on Biomedical Engineering*, 66(3):689–694, 2018.
- [Chaudhary et al.(2022)Chaudhary, Gerard, Wang, Christensen, Cooper, Schroeder, Hoffman, and Reinhardt] Muhammad FA Chaudhary, Sarah E Gerard, Di Wang, Gary E Christensen, Christopher B Cooper, Joyce D Schroeder, Eric A Hoffman, and Joseph M Reinhardt. Single volume lung biomechanics from chest computed tomography using a mode preserving generative adversarial network. In *2022 IEEE 19th International Symposium on Biomedical Imaging (ISBI)*, pages 1–5. IEEE, 2022.
- [Zhang et al.(2022b)Zhang, Zhao, Bao, Li, Qian, Frangi, Xie, and Zhang] Jie Zhang, Yihui Zhao, Tianzhe Bao, Zhenhong Li, Kun Qian, Alejandro F Frangi, Sheng Quan Xie, and Zhi-Qiang Zhang. Boosting personalised musculoskeletal modelling with physics-informed knowledge transfer. *IEEE Transactions on Instrumentation and Measurement*, 2022b.
- [Nasr et al.(2021)Nasr, Bell, He, Whittaker, Jiang, Dickerson, and McPhee] Ali Nasr, Sydney Bell, Jiayuan He, Rachel L Whittaker, Ning Jiang, Clark R Dickerson, and John McPhee. Muscletnet: mapping electromyography to kinematic and dynamic biomechanical variables by machine learning. *Journal of Neural Engineering*, 18(4):0460d3, 2021.
- [Solares et al.(2020)Solares, Raimondi, Zhu, Rahimian, Canoy, Tran, Gomes, Payberah, Zottoli, Nazarzadeh, et al.] Jose Roberto Ayala Solares, Francesca Elisa Diletta Raimondi, Yajie Zhu, Fatemeh Rahimian, Dexter Canoy, Jenny Tran, Ana Catarina Pinho Gomes, Amir H Payberah, Mariagrazia Zottoli, Milad Nazarzadeh, et al. Deep learning for electronic health records: A comparative review of multiple deep neural architectures. *Journal of biomedical informatics*, 101:103337, 2020.
- [Shadlen et al.(1996)Shadlen, Britten, Newsome, and Movshon] Michael N Shadlen, Kenneth H Britten, William T Newsome, and J Anthony Movshon. A computational analysis of the relationship between neuronal and behavioral responses to visual motion. *Journal of Neuroscience*, 16(4):1486–1510, 1996.
- [Holder et al.(2020)Holder, Trinler, Meurer, and Stief] Jana Holder, Ursula Trinler, Andrea Meurer, and Felix Stief. A systematic review of the associations between inverse dynamics and musculoskeletal modeling to investigate joint loading in a clinical environment. *Frontiers in bioengineering and biotechnology*, 8:603907, 2020.
- [Hu et al.(2022)Hu, Chapman, Wen, and Hall] Yang Hu, Adriane Chapman, Guihua Wen, and Dame Wendy Hall. What can knowledge bring to machine learning?—a survey of low-shot learning for structured data. *ACM Transactions on Intelligent Systems and Technology (TIST)*, 13(3):1–45, 2022.
- [Tam et al.(2022)Tam, Boukadoum, Campeau-Lecours, and Gosselin] Simon Tam, Mounir Boukadoum, Alexandre Campeau-Lecours, and Benoit Gosselin. Siamese convolutional neural network and few-shot learning for embedded gesture recognition. In *2022 20th IEEE Interregional NEWCAS Conference (NEWCAS)*, pages 114–118. IEEE, 2022.

- [Rahimian et al.(2021a)Rahimian, Zabihi, Asif, Atashzar, and Mohammadi] Elahe Rahimian, Soheil Zabihi, Amir Asif, S Farokh Atashzar, and Arash Mohammadi. Trustworthy adaptation with few-shot learning for hand gesture recognition. In *2021 IEEE International Conference on Autonomous Systems (ICAS)*, pages 1–5. IEEE, 2021a.
- [Rahimian et al.(2021b)Rahimian, Zabihi, Asif, Farina, Atashzar, and Mohammadi] Elahe Rahimian, Soheil Zabihi, Amir Asif, Dario Farina, Seyed Farokh Atashzar, and Arash Mohammadi. Fs-hgr: Few-shot learning for hand gesture recognition via electromyography. *IEEE transactions on neural systems and rehabilitation engineering*, 29:1004–1015, 2021b.
- [Lehmler et al.(2022)Lehmler, Saif-ur Rehman, Tobias, and Iossifidis] Stephan Johann Lehmler, Muhammad Saif-ur Rehman, Glasmachers Tobias, and Ioannis Iossifidis. Deep transfer learning compared to subject-specific models for semg decoders. *Journal of Neural Engineering*, 19(5):056039, 2022.
- [Goodfellow(2014)] Ian J Goodfellow. On distinguishability criteria for estimating generative models. *arXiv preprint arXiv:1412.6515*, 2014.
- [Goodfellow et al.(2020)Goodfellow, Pouget-Abadie, Mirza, Xu, Warde-Farley, Ozair, Courville, and Bengio] Ian Goodfellow, Jean Pouget-Abadie, Mehdi Mirza, Bing Xu, David Warde-Farley, Sherjil Ozair, Aaron Courville, and Yoshua Bengio. Generative adversarial networks. *Communications of the ACM*, 63(11):139–144, 2020.
- [Shi et al.(2022)Shi, Han, Han, Chang, Hu, and Dancey] Yue Shi, Liangxiu Han, Lianghao Han, Sheng Chang, Tongle Hu, and Darren Dancey. A latent encoder coupled generative adversarial network (le-gan) for efficient hyperspectral image super-resolution. *IEEE Transactions on Geoscience and Remote Sensing*, 60:1–19, 2022.
- [Chen et al.(2022)Chen, Qian, Wang, and Fang] Zihan Chen, Yaojia Qian, Yuxi Wang, and Yinfeng Fang. Deep convolutional generative adversarial network-based emg data enhancement for hand motion classification. *Frontiers in Bioengineering and Biotechnology*, 10:909653, 2022.
- [Fahimi et al.(2020)Fahimi, Dosen, Ang, Mrachacz-Kersting, and Guan] Fatemeh Fahimi, Strahinja Dosen, Kai Keng Ang, Natalie Mrachacz-Kersting, and Cuntai Guan. Generative adversarial networks-based data augmentation for brain–computer interface. *IEEE transactions on neural networks and learning systems*, 32(9):4039–4051, 2020.
- [Zhao et al.(2022b)Zhao, Yu, Wang, Ma, Sheng, and Zhu] Jiamin Zhao, Yang Yu, Xu Wang, Shihan Ma, Xinjun Sheng, and Xiangyang Zhu. A musculoskeletal model driven by muscle synergy-derived excitations for hand and wrist movements. *Journal of Neural Engineering*, 19(1):016027, 2022b.
- [Yu et al.(2017)Yu, Zhang, Wang, and Yu] Lantao Yu, Weinan Zhang, Jun Wang, and Yong Yu. Seqgan: Sequence generative adversarial nets with policy gradient. In *Proceedings of the AAAI conference on artificial intelligence*, volume 31, 2017.
- [Han et al.(2019)Han, Zhou, Geng, Chen, Wang, and Wei] Yongming Han, Rundong Zhou, Zhiqiang Geng, Kai Chen, Yajie Wang, and Qin Wei. Production prediction modeling of industrial processes based on bi-1stm. In *2019 34th Youth Academic Annual Conference of Chinese Association of Automation (YAC)*, pages 285–289. IEEE, 2019.
- [Nah et al.(2017)Nah, Hyun Kim, and Mu Lee] Seungjun Nah, Tae Hyun Kim, and Kyoung Mu Lee. Deep multi-scale convolutional neural network for dynamic scene deblurring. In *Proceedings of the IEEE conference on computer vision and pattern recognition*, pages 3883–3891, 2017.
- [Wu et al.(2020)Wu, Liu, and Wang] Hongping Wu, Yuling Liu, and Jingwen Wang. Review of text classification methods on deep learning. *Comput. Mater. Contin*, 63(3):1309–1321, 2020.
- [Srivastava et al.(2015)Srivastava, Greff, and Schmidhuber] Rupesh Kumar Srivastava, Klaus Greff, and Jürgen Schmidhuber. Highway networks. *arXiv preprint arXiv:1505.00387*, 2015.
- [Liu et al.(2008)Liu, Anderson, Schwartz, and Delp] May Q Liu, Frank C Anderson, Michael H Schwartz, and Scott L Delp. Muscle contributions to support and progression over a range of walking speeds. *Journal of biomechanics*, 41(15):3243–3252, 2008.
- [Zhang et al.(2016)Zhang, Ding, and Zhang] Nan Zhang, Shifei Ding, and Jian Zhang. Multi layer elm-rbf for multi-label learning. *Applied soft computing*, 43:535–545, 2016.
- [Solnik et al.(2008)Solnik, DeVita, Rider, Long, and Hortobágyi] Stanisław Solnik, Paul DeVita, Patrick Rider, Benjamin Long, and Tibor Hortobágyi. Teager–kaiser operator improves the accuracy of emg onset detection independent of signal-to-noise ratio. *Acta of bioengineering and biomechanics/Wroclaw University of Technology*, 10(2):65, 2008.
- [Kahl and Hofmann(2016)] Lorenz Kahl and Ulrich G Hofmann. Comparison of algorithms to quantify muscle fatigue in upper limb muscles based on semg signals. *Medical Engineering & Physics*, 38(11):1260–1269, 2016.



---

[Pan et al.(2022)Pan, Liu, and Li] Lizhi Pan, Kai Liu, and Jianmin Li. Effect of subcutaneous muscle displacement of flexor carpi radialis on surface electromyography. *IEEE Transactions on Neural Systems and Rehabilitation Engineering*, 30:1244–1251, 2022.

[Jung and Keuper(2021)] Steffen Jung and Margret Keuper. Internalized biases in fréchet inception distance. In *NeurIPS 2021 Workshop on Distribution Shifts: Connecting Methods and Applications*, 2021.